A Lagrangian interpolation-assisted direct laser absorption spectrum analyzer based on digital signal processor for methane detection

Di Yu[1] · Yanwen Zhou[1] · Fang Song[1] · Weilin Ye[2] · Yue Yang[1] · Yu Zhang[1] · Yiding Wang[1] · Chuantao Zheng[1] · Frank K. Tittel[3]

Abstract

A novel Lagrangian interpolation-based direct laser absorption spectroscopy (LI-DLAS) technique was presented to suppress noise in infrared gas detection by incorporating Lagrangian interpolation and nonlinear least-square fitting (NLLSF). An LI-DLAS analyzer was reported for methane (CH_4) detection using a 1654 nm distributed feedback (DFB) laser, a compact digital signal processor (DSP), and a multi-pass gas cell (MPGC) with a 16 m optical path length. The performance of the developed LI-DLAS CH_4 analyzer was evaluated by means of laboratory experiments. Compared with the traditional DLAS-based sensor without Lagrangian interpolation, the detection sensitivity was improved from 6 ppmv to 2 ppmv, and the detection stability was enhanced as the Allan–Werle deviation was dropped from 1.514 to 0.531 ppmv for a 1 s averaging time. Compared with a DLAS analyzer based on LabVIEW platform, the DSP-based CH_4 analyzer shows the merits of compact size and low cost with potential filed-deployable applications in industrial monitoring and control.

1 Introduction

Methane (CH_4), the second worldwide greenhouse gas after carbon dioxide (CO_2), has a 25 times enhancement compared to the global warming potential of CO_2 [1]. Hence, atmospheric CH_4 monitoring is significant for the observation and analysis of the climate trends [2–4]. Besides, as an inflammable gas, CH_4 leakage during the exploration and transportation of natural gas is a vital safety hazard [5, 6]. Therefore, CH_4 detection has received considerable attention in industrial process control [7–9]. Among the existing CH_4 detection techniques, infrared laser absorption spectroscopy has wide industrial and academic applications owing to their high-precision sensing capability and fast response [10, 11].

Tunable diode laser absorption spectroscopy (TDLAS) is a mature technique extensively developed in CH_4 detection for high sensitivity, long-term stability, and fast response [12]. There are two well-established methods derived from TDLAS: wavelength modulation spectroscopy (WMS) [13] and direct laser absorption spectroscopy (DLAS) [14]. WMS requires frequent sensor calibration, which makes the sensor structure and signal processing procedure complicated. On the contrary, DLAS has the ability to offer quantitative concentration directly from the relative change in light intensity according to Beer–Lambert law, resulting in a much simplified system structure [15]. To avoid interference from other absorption lines and to improve detection accuracy, DLAS requires a tunable laser source with single-frequency emission and a narrow line width at the target absorption line of a gas molecule. Considering that the fabrication technology of a near-infrared (NIR) semiconductor laser is mature and an NIR laser source can be easily fiber-coupled, a continuous-wave (CW) NIR-distributed feedback (DFB) laser is an attractive choice for the development of DLAS-based gas sensors [16, 17].

However, DLAS possesses the inherent drawbacks of being highly susceptible to the noise across a large bandwidth, especially the low-frequency noise due to its simple data processing procedure [18]. To improve the signal-to-noise ratio (SNR) and detection accuracy, apart from

✉ Weilin Ye
  wlye@stu.edu.cn

✉ Chuantao Zheng
  zhengchuantao@jlu.edu.cn

1 State Key Laboratory of Integrated Optoelectronics, College of Electronic Science and Engineering, Jilin University, 2699 Qianjin Street, Changchun 130012, China

2 College of Engineering, Shantou University, 243 Daxue Road, Shantou 515063, China

3 Department of Electrical and Computer Engineering, Rice University, 6100 Main Street, Houston, TX 77005, USA

reducing the interference from optical path, some effective data processing algorithms can be adopted [19, 20]. In our previously reported traditional DLAS systems, besides the nonlinear absorption line fitting, a sliding average filtering was performed to suppress the electrical-domain background noise and interference [2, 8]. However, this data processing method averages the measured data and, thus, probably changes the signal's statistical characteristics.

For noise suppression, we developed an alternative technique by introducing Lagrangian interpolation (LI) [21] into DLAS technique. Considering the fact that the noise point exhibits an even or odd symmetry, a filtering range was set by means of the mathematical model of Beer–Lambert law, and then, the filtered data were recovered by LI. After that, the gas concentration was retrieved from the processed data by the real-time nonlinear least-square fitting of the interpolated signal to an absorption line profile, which were widely used in baseline fitting and absorption line fitting [2, 14]. To meet the needs of mobile and field-deployable gas measurements, a compact gas sensor system should be available. In this work, an LI-DLAS analyzer for CH_4 detection was realized based on a compact digital signal processor (DSP) board with low-power consumption. Compared to our reported LabVIEW-based system for DLAS CH_4 detection [3, 22], the DSP-based CH_4 analyzer has a lower

power-budget and realizes miniaturization in electrical system. The LI-DLAS CH_4 sensing performance was evaluated by laboratory measurements, which was enhanced in terms of sensitivity and stability compared with a traditional DLAS-based CH_4 analyzer without such data processing.

2 Structure and design of the LI-DLAS CH_4 analyzer

2.1 Selection of CH_4 absorption line and optical source

According to the high-resolution transmission (HITRAN) molecular absorption database [23], the CH_4 absorption line located at 6046.965 cm^{-1} is the strongest absorption line in the near-infrared $2\nu_3$ absorption band, as shown in Fig. 1a. Simultaneously, the absorbance of 2% H_2O and 100 ppmv CH_4 in Fig. 1b indicates that absorption strength of H_2O is much less than CH_4's, and could be omitted [24]. Hence, the NIR absorption line at 6046.96 cm^{-1}, whose detailed information is listed in Table 1, was selected as the target line. The DFB laser emitting at a center wavenumber of 6046.95 cm^{-1} with an output power of 5.5 mW requires an operation temperature of 17 °C and a driving current of
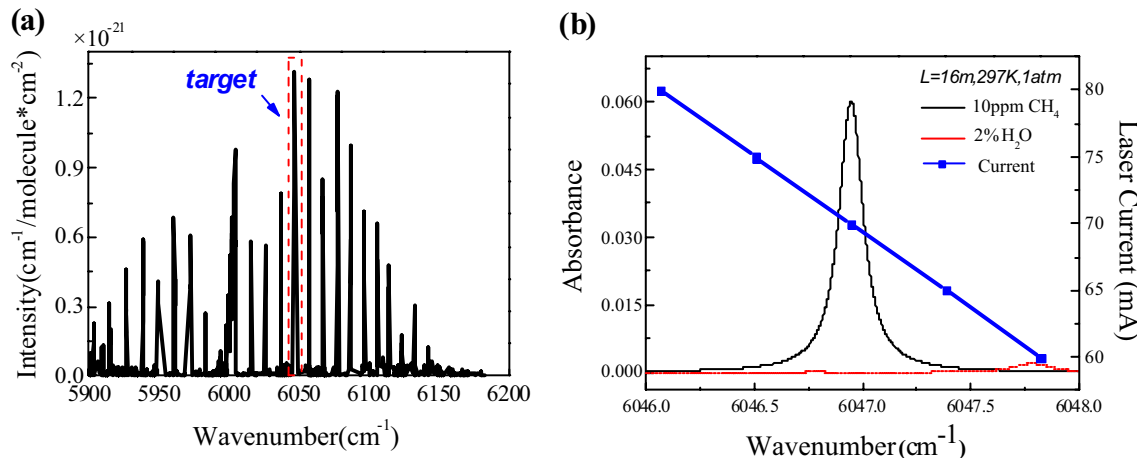
Fig. 1 HITRAN-based absorption spectra of **a** CH_4 from 5900 to 6200 cm^{-1}, and **b** 100 ppmv CH_4 and 2% H_2O at a pressure of 1 atm, an effective optical path length of 1600 cm and a temperature of 297 K. **b** DFB laser emission wavenumber as a function of the driver current at a laser operation temperature of 17 °C

Table 1 Detailed information of the CH_4 absorption line at 6046.96 cm^{-1}

Isotopologue	v_0 (cm^{-1})	S (cm^{-1} $(mo\ cm^{-2})^{-1}$)	γ_{air} (cm^{-1} atm^{-1})	γ_{self} (cm^{-1} atm^{-1})	n_{air}
$^{12}CH_4$	6046.9647	1.335×10^{-21}	0.0621	0.082	0.85

Parameters are cited from HITRAN2012 database [23]

v_0 center frequency, S line strength, γ_{air} air broadening factor, γ_{self} self-expansion coefficient, n_{air} temperature coefficient

70.0 mA. According to the linear relation between the DFB laser emitting wavenumber and driving current shown in Fig. 1b, the current range was decided to be 55.5–83.0 mA at an operation temperature of 17 °C to scan the CH_4 line.

2.2 LI-DLAS analyzer structure

The structure of the DSP-based LI-DLAS analyzer for CH_4 detection is depicted in Fig. 2, consisting of an optical and an electrical part. In the optical part (Fig. 2a), a CW NIR butterfly packaged DFB laser (Sichuan Bolian Photonics Technology, China) was used to target the CH_4 absorption line at 1.654 µm. The laser beam was collimated and coupled to a multi-pass gas cell with an effective optical path length of 16 m (physical size: $290 \times 90 \times 80$ mm^3, Liujiu Sensing Technology, Wuhan, China). After passing through the cell, the output laser beam was focused onto an InGaAs photodetector which generated an electrical signal.

As shown in Fig. 2b, the electrical part includes a temperature controller (TED200C, Thorlabs, USA), an integrated laser current driver (LDC202C, Thorlabs, USA), and a DSP-based direct laser absorption signal processor with a dimension size of 10.0×6.1 cm^2. The used DLAS technique for CH_4 detection only requires a saw tooth scan signal. This scan signal was generated by a direct digital synthesizer (DDS) module (model #AD9834). The detector signal output from the InGaAs photodetector was sent to the DSP for data processing. The processed absorption signal was recorded and displayed on a liquid crystal display

(LCD) screen and also could be delivered to a laptop via an UART port for post-data analysis. The supply voltage and power consumption of the compact DSP board are ± 12 V and ~3.612 W, respectively. In addition, a pressure controller (model 649, MKS Instruments, USA) and a vacuum pump (N838.3 KN.18, KNF, Germany) were used to control and maintain the pressure inside the MPGC.

2.3 Absorption fundamental

The absorption of a target gas specie can be determined by measuring the attenuation of light intensity when light transmits through the gas, as defined by the Beer–Lambert law [25]:

$$I(v) = I_0(v) \exp \left[-PcS(T)\phi(v)L \right], \qquad (1)$$

where v (cm^{-1}) is the laser frequency, $I(v)$ and $I_0(v)$ are the transmitted laser light intensity with and without the presence of the target absorbers, respectively, P(atm) is the gas pressure, c is the mole fraction of the gas, $S(T)$ (cm^{-2} atm^{-1}) is the absorption line intensity at temperature T, $\phi(v)$ (cm) is the line-shape function, and L (cm) is the absorption path length.

A polynomial was used to fit the transmitted laser light intensity $I(v)$ to generate a baseline $I_b(v)$ (the detailed fitting method can be seen in Sect. 3.1), which is considered as the background light intensities $I_0(v)$. Then, the absorbance $\alpha(v)$ can be expressed by the following equation:
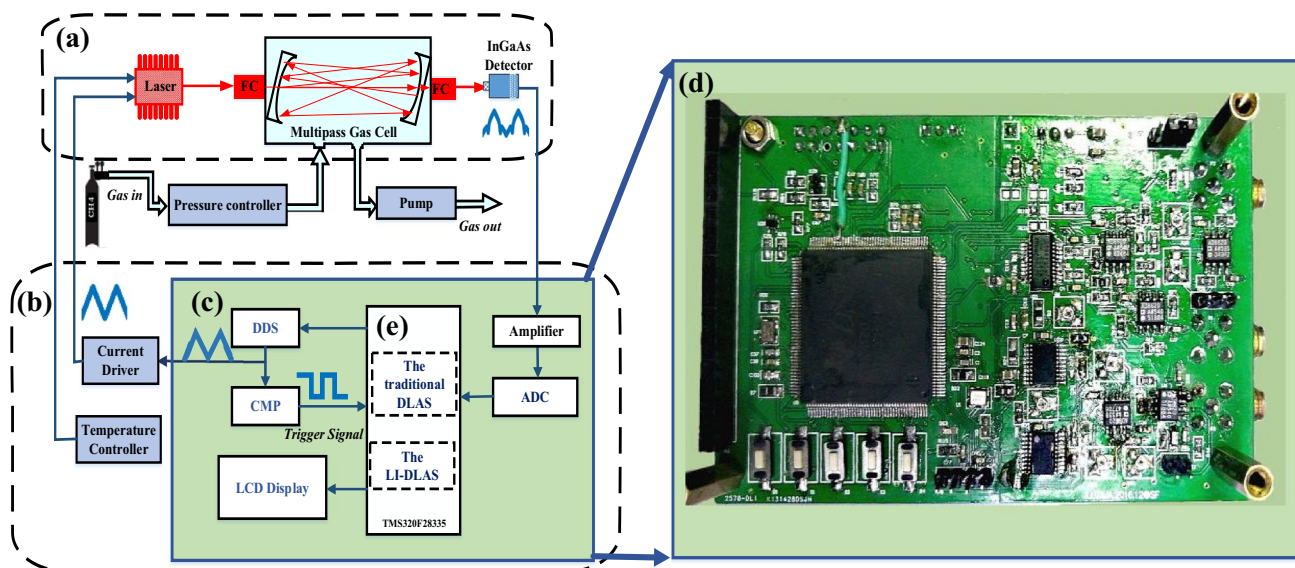
Fig. 2 Schematic illustration of the LI-DLAS analyzer for CH_4 detection, **a** the optical part, **b** the electrical part, **c** the DSP platform for data processing, and **d** the photograph of the DSP-based DLAS board. *FC* fiber collimator, *CMP* comparators, *CE* concentration extraction, *ADC* analog-to-digital converter

$$\alpha(v) = -\ln\left[I(v)/I_0(v)\right] = \ln\left[I_b(v)/I(v)\right] = PcS(T)\phi(v)L. \tag{2}$$

The linear function $\phi(v)$ is related to pressure, temperature, composition, and diagnostic wavelength. The line type function $\phi(v)$ can take three different form of function: Gaussian, Lorentzian, and Voigt [26, 27].

2.4 Line-shape function selection

The DLAS analyzer was operated at an atmospheric pressure (1 atm) and room temperature (296 K). The spectroscopic models with an NIR absorption line at 1.654 μm under this operation condition are shown in Fig. 3 [24]. Since the selected model of the absorption line has a direct effect on filtering parameters, the quantitative measurement of CH_4 concentration requires a more refined spectral model. As shown in Fig. 3,
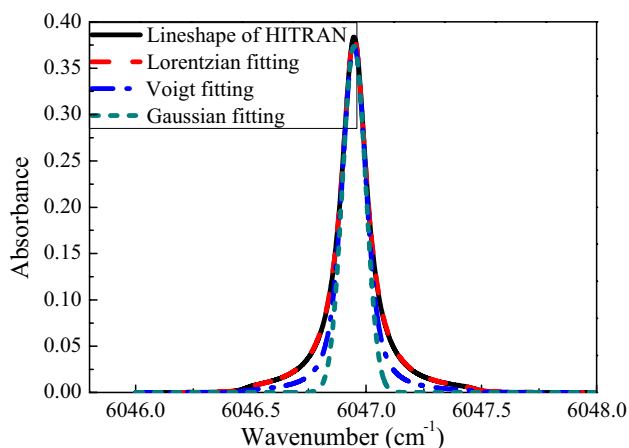
Fig. 3 The CH_4 absorption line at 6046.95 cm^{-1} recorded at $P = 1$ atm, $T = 297$ K, $L = 16$ m, $C = 650$ ppmv, and the three fitting line profiles

a validation of HITRAN 2012 yielded a generally good agreement with the Lorentzian profile fitting in the [6046.0 cm^{-1}, 6048.0 cm^{-1}] range at 296 K and 1 atm. $\phi(v)$ can be expressed as a Lorentzian line-shape function, written as follows:

$$\phi(v) = \frac{\Delta v_L}{\pi}\left[\frac{1}{\left(v - v_0\right)^2 + \Delta v_L^2}\right]. \tag{3}$$

Here, Δv_L is the half width at the half maximum (HWHM), and v_0 is the central wavenumber of the absorption line [28].

3 LI-DLAS technique

The traditional DLAS technique used in CH_4 detection is shown in Fig. 4a, which requires a baseline fitting (BF) algorithm to get the background signal without a reference channel and a nonlinear least-square fitting (NLLSF) to obtain the CH_4 absorbance for concentration determination. The sensitivity of traditional DLAS is limited by low-frequency noise, and therefore, an improved LI-DLAS technique is proposed to improve the measurement precision. As shown in Fig. 4b, the LI-DLAS technique includes three steps: BF based on least-square fitting (LSF), data processing algorithm based on LI, and NLLSF of absorption line profile.

3.1 Background fitting

A periodic triangular signal generated by the DDS module is used to adjust the output wavelength of the DFB laser, which can be expressed as follows:

Fig. 4 Function diagram of the DSP-based **a** traditional DLAS and **b** LI-DLAS data processing system. *CE* concentration extraction
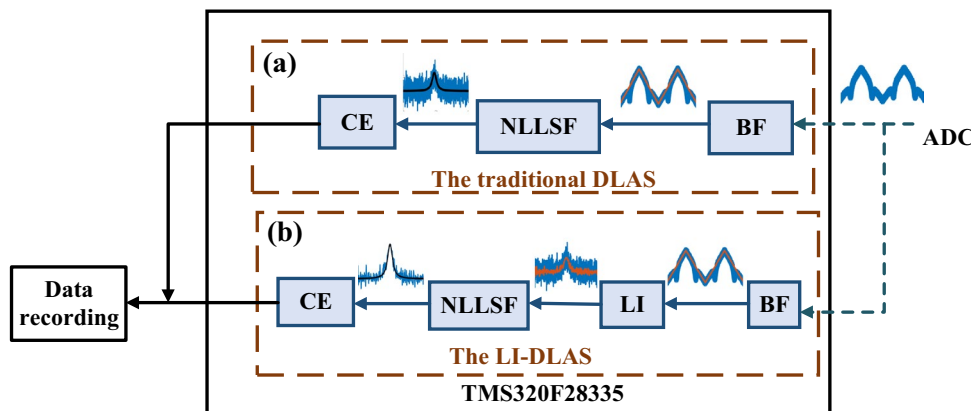
$$u(t) = \begin{cases} -kA_{\text{tri}} + \left(2A_{\text{tri}}/T_{\text{tri}}\right)t, \ kT_{\text{tri}} \le t \le (2k+1)T_{\text{tri}}/2 \\ 2(k+1)A_{\text{tri}} - \left(2A_{\text{tri}}/T_{\text{tri}}\right)t, \ (2k+1)T_{\text{tri}}/2 \le t \le (k+1)T_{\text{tri}} \end{cases}, \quad k = 0, 1, 2 \dots, \tag{4}$$

where A_{tri} and T_{tri} are the amplitude and the period of the scan signal, respectively. Without gas absorption, the laser optical intensity $I_{\text{b}}(t)$ received by the InGaAs detector is as follows:

$$I_{\text{b}}(t) = I_0[1 + mu(t)], \tag{5}$$

where I_0 is the laser output optical intensity and m is the light intensity modulation coefficient. According to Eqs. (1) and (5), the electrical signal u_{r} generated and amplified by the photoelectric detector can be expressed as follows:

$$u_{\text{r}}(t) = KD_{\text{oe}}I_0[1 + mu(t)] \exp\left[-PcS(T)\phi(t)L\right], \tag{6}$$

where K is the amplifying factor and D_{oe} is the photoelectric conversion parameters.

The transmitted laser light intensities in the [6046.0, 6046.5] cm^{-1} and the [6047.5, 6048] cm^{-1} region were extracted and fitted by applying a polynomial to generate a spectral baseline, which is considered as the background light intensity. Divide the CH_4 absorption band [6046 cm^{-1}, 6048 cm^{-1}] into N subbands with a length of $h = 1/N$ cm^{-1} each, and define $x_i = 6046 + ih(i = 1,2,…,N)$. Then, the polynomial expression $u_{\text{b}} = k_1x + k_2$ is considered as the mathematical expression of background signal, where k_1 and k_2 can be calculated according to the following equation:

$$\begin{cases} Nk_2/2 + k_1 \left(\sum_{i=1}^{N/4} x_i + \sum_{i=3N/4+1}^{N} x_i \right) = \sum_{i=1}^{N/4} u_{\text{r}}(i) + \sum_{i=3N/4+1}^{N} u_{\text{r}}(i) \\ k_2 \left(\sum_{i=1}^{N/4} x_i + \sum_{i=3N/4+1}^{N} x_i \right) + k_1 \left(\sum_{i=1}^{N/4} x_i^2 + \sum_{i=3N/4+1}^{N} x_i^2 \right) = \sum_{i=1}^{N/4} x_i u_{\text{r}}(i) + \sum_{i=3N/4+1}^{N} x_i u_{\text{r}}(i) \end{cases}. \tag{7}$$

3.2 Data processing algorithm based on Lagrangian interpolation

Given the systematic and random noise of the DLAS, it is necessary to use a simple and fast algorithm for data processing. Let $y(x) = 1/\ln(u_{\text{b}}(x)/u(x)) = 1/\alpha(x)$, and the second-order differential equation of $y''(x_i)$ will be the following:

$$y''(x_i) = \lim_{h \to 0} \left[\frac{y(x_{i+1}) - y(x_i)}{h^2} - \frac{y(x_i) - y(x_{i-1})}{h^2} \right]$$
$$= 2\pi \big/ \left(PcLS(T)\Delta v_{\text{L}} \right), \tag{8}$$

where $2\pi/(PcLS(T)\Delta v_{\text{L}})$ is a definite value. Then, we set a constant as a threshold for filtering. Replace the derivatives by the second-order finite-difference S_i [29]:

$$S_i = 2y(x_i) - \left[y(x_{i+1}) + y(x_{i-1}) \right]. \tag{9}$$

Then, Eq. (8) can be re-written as follows:

$$y''(x_i) = \lim_{\Delta v \to 0} \left(\frac{-S_i}{h^2} \right). \tag{10}$$

Define $\bar{S}$ as the average value of the array $\{S_i\}$, and Eq. (11) can be obtained as the following form:

$$\bar{S} = \frac{1}{N-1} \sum_{i=1}^{N-1} S_i = \left[y(x_1) - y(x_0) + y(x_{N-1}) - y(x_N) \right] \big/ (N-1). \tag{11}$$

Note that $\bar{S}$ only relates to the edge data. From a long-term monitoring of $|S_i - \bar{S}|_{\text{normal}}$ for the normal data points and $|S_i - \bar{S}|_{\text{abnormal}}$ for the abnormal data points, we can derive a statistical threshold value W_1 to distinguish the normal and abnormal data points. That is to say, when a data point satisfies $|S_i - \bar{S}| > W_1$, it is abnormal; otherwise, it is normal.

The selected data at the ith deposition should be processed to minimize the distortion of the recovered data. An LI function was used to obtain the predictive values. The interpolation data $L_2(x_i)$ of the three data points near (x_i, y_i) can be regarded as the ith predictive value, which is written as follows:

$$L_2(x_i) = \sum_{k=m}^{m+3} y(x_k) \prod_{\substack{j=m \\ j \ne k}}^{m+3} \left[(x - x_j) \big/ (x_k - x_j) \right] \ (m = i-2, m \ne i). \tag{12}$$

Besides, the data estimated by the above method may be far from the true data due to spikes and interference of abrupt noise. Therefore, the interpolation point is modified by adding another judging criteria W_2 for preserving more information from the measured data. Then, we have the following:

$$y(x) = \begin{cases} L_2(x_i), \left| y(x_i) - L_2(x_i) \right| \ge W_2 \\ y(x_i), \left| y(x_i) - L_2(x_i) \right| < W_2 \end{cases}. \tag{13}$$

The corresponding limit can be evaluated as $W_2 = 2\left(y_{\max} - y_{\min}\right)\big/N$.

3.3 Nonlinear least-square fitting of absorption line profile

The line-shape function $\phi(v)$ is determined by the line profile. The data perturbed by random noise can be fixed by

means of an NLLSF. A regression function $f(x)$ represents the fitting formula $y(x)$ as follows:

$$f(x) = \sum_{k=0}^{2} p_k \varphi_k(x), \tag{14}$$

where p_k is the fitting parameters, and $\varphi_k(x) = x^k$. The key issue is to build the profile fit with correct parameters p_k. Let $\boldsymbol{P} = [p_0, p_1, p_2]$, and the n-dimensional nonzero vectors $\varphi_k(x_s) = x_s^k$. Define a matrix $\boldsymbol{A}$ and vectors $\boldsymbol{b}$, which satisfies the following:

$$\mathbf{AP} = \mathbf{b}, \tag{15}$$

where the elements a_{ij} in matrix $\boldsymbol{A}$ becomes $a_{ij} = \boldsymbol{\varphi}_i \cdot \boldsymbol{\varphi}_j^{\mathrm{T}}$ and the elements b_j in vectors $\boldsymbol{b}$ is $b_i = \boldsymbol{\varphi}_i \cdot \mathbf{y}$. $\boldsymbol{A}$ is a positive definite matrix because a_{ij} is equal to a_{ji}. For reducing the calculation complexity, $\boldsymbol{A}$ can be decomposed into a lower triangular matrix $\boldsymbol{L}$ and a transpose of $\boldsymbol{L}$:

$$\mathbf{A} = \mathbf{LL}^{\mathrm{T}}. \tag{16}$$

The element l_{ij} of matrix $\boldsymbol{L}$ becomes the following:

$$l_{ij} = \begin{cases} \left(a_{ij} - \sum_{k=1}^{j-1} l_{ik} l_{jk}\right) \Big/ l_{jj} (i \neq j) \\ \sqrt{a_{jj} - \sum_{k=1}^{j-1} l_{jk}^2} (i = j) \end{cases}. \tag{17}$$

Supposing that $\mathbf{LT} = \mathbf{b}$ and $\mathbf{L}^{\mathrm{T}}\mathbf{P} = \mathbf{T}$, the elements of $\mathbf{T}$ can be described as $t_k = \dfrac{b_k - \sum_{j=1}^{k-1} l_{jk} t_j}{l_{kk}}$. The optimal coefficient is determined as $p_k = \dfrac{t_k - \sum_{j=1}^{n} l_{jk} x_j}{l_{kk}}$. Then, the regression function $f(x)$ can be achieved for the inversion of CH_4 concentration.

3.4 LI-DLAS technique evaluation

As shown in Fig. 5, the developed analyzer was used to detect CH_4 (1 atm, 297 K, 16 m, 10 ppmv) for evaluating the data processing performance of the LI-DLAS algorithm. The scan signal was a triangular signal with a variation range from ~1.2 V to ~2.8 V and a frequency of 1 Hz. The first half-period (rising part) of the detector signal was sampled and was processed at the second half-period (downing part). The two wings of the sample signal were extracted and the BF algorithm was used to get the baseline, which is shown in Fig. 5b. Subsequently, the background signal was removed from the absorption signal, resulting in an absorbance signal, as shown in Fig. 5c. In the traditional DLAS sensor, the absorbance curve is obtained directly using NLLSF as depicted in Fig. 5d. The subgraph of Fig. 5d shows that there is a big difference

between the fitted and theoretical absorbance curve, which affects the concentration retrieval. The processed data obtained using the LI algorithm to effectively decrease the noise is shown in Fig. 5e. It can be seen from the subgraph in Fig. 5f that the fitted absorption curve obtained almost coincides with the theoretical curve, which confirms the denoising operation of the LI-DLAS algorithm.

3.5 Detection procedure and software

We compiled a C program for the DSP processor (TMS320F28335) using CCS 6.0 platform. The entire program can be overviewed by a flowchart in Fig. 6. The flowchart illustrates the logic of the developed LI-DLAS algorithm, in comparison with a traditional DLAS method (i.e., the flowchart without the program contained in dashed box).
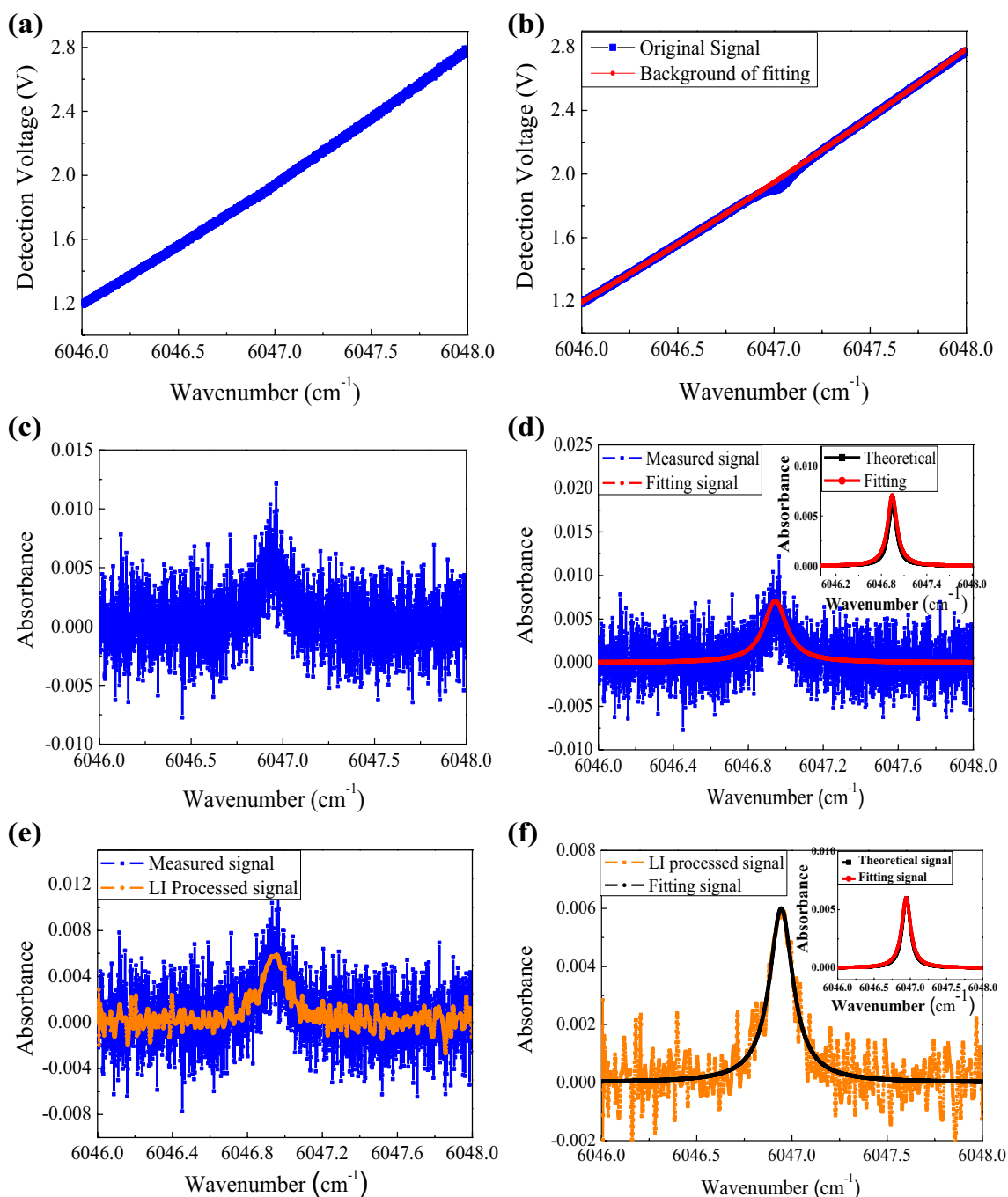
4 Application of the LI-DLAS analyzer for CH_4 sensing

4.1 Absorbance measurements

A multi-component gas mixing system (Environics 4000, Environics, USA) was used to prepare CH_4 samples with eight concentration levels of 26, 27, 28, 30, 32, 38, 52, and 74 ppmv by mixing a standard 100 ppmv CH_4 sample and pure nitrogen (N_2). Each sample was tested for ~10 min. The amplitude of the normalized absorbance signal ($u_{\mathrm{absorbance}}(t) = -\ln\left(u(t)/u_{\mathrm{b}}(t)\right)$) for each concentration is plotted in Fig. 7a. The relationship between the measured concentration and the theoretical CH_4 concentration is shown in Fig. 7b. The fitting curve indicates that the measured concentration is basically equal to the theoretical concentration.

4.2 Detection sensitivity

To show the superiority of the algorithm proposed in Sect. 3, we carried out an experiment with and without the algorithm. The minimum concentration change that can be distinguished by the analyzer is defined as detection sensitivity. The gas cell was first filled with pure N_2, and then, a standard 100 ppmv CH_4 sample was injected. To observe the detection performance, we obtained 60 absorbance peak readings for each gas sample and the detected amplitudes are shown in Fig. 8. The measurement results without data processing algorithm are shown in Fig. 8a. The variation ranges of the detected amplitude under 27.5, 27, 28, 30, and 32 ppmv are overlapped. In addition, there are some abnormal concentration data dots during measurement. This can be attributed to the absorption line fitting error because of the
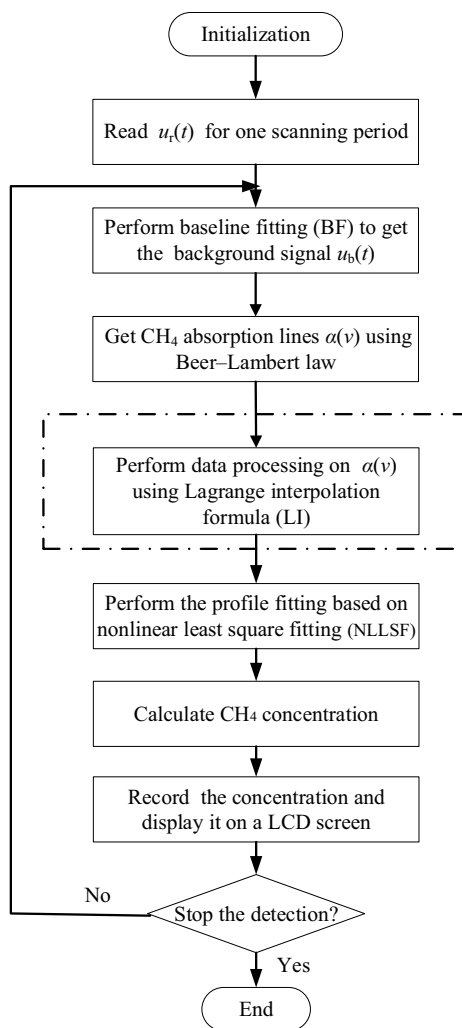
Fig. 5 Data processing based on the LI-DLAS analyzer for the detection of the CH_4 sample with a concentration level of 10 ppmv. **a** The output signal from the detector with no absorption. **b** The output signal from the detector and its baseline fitting for a 10 ppmv CH_4 sample. **c** The measured ab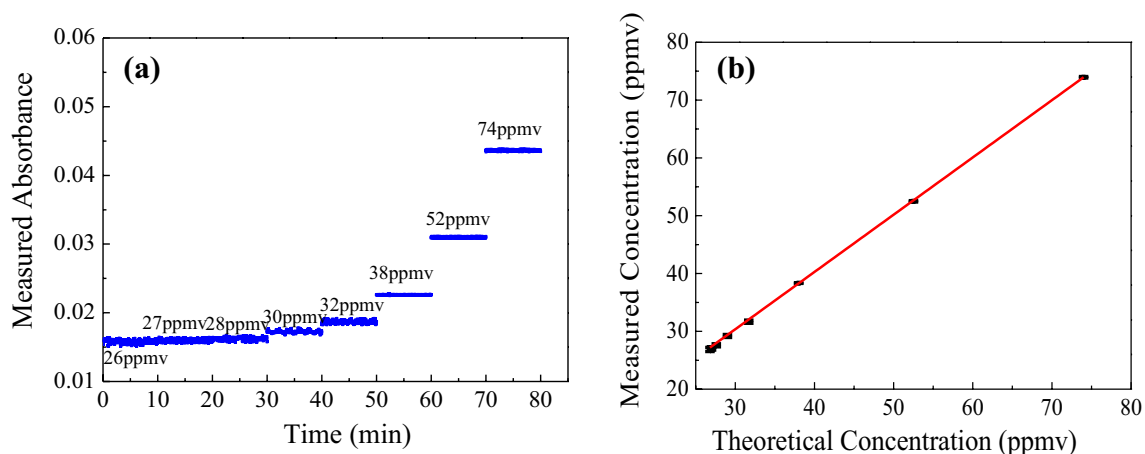sorbance curve and **d** the fitting curve of the measured signal using the traditional DLAS, where the subgraph shows the fitted absorbance curve and the theoretical curve. **e** The LI-processed absorbance signal and **f** the fitting curve of LI-processed signal, where the subgraph shows the fitted absorbance curve and the theoretical curve

abnormal data point in the absorption signal. After removing these abnormal data points using LI, Fig. 8b shows reduced overlap in the detected amplitude and no abnormal concentration data dots. The minimum detected amplitude at 28 ppmv is larger than the maximum detected amplitude under

26.5 ppmv. It means that, under certain concentration, the detection sensitivity using a traditional method was about 6 ppmv (Fig. 8a), while the detection sensitivity is decided to be about 2 ppmv using the developed algorithm (Fig. 8b).

4.3 Allan variance and detection stability

To examine the long-term stability of the developed LI-DLAS analyzer, long-term measurement of a 4 ppmv CH_4 sample was carried out for ~ 2 h. The measured concentration results without using the algorithm and using the algorithm were recorded and are exhibited in Figs. 9a and 10a, respectively. A histogram plot was used to observe the distribution of the measured concentration, as shown in the insets of Figs. 9b and 10b, respectively. The Allan–Werle deviation plots obtained from the time-series measurement result in Figs. 9a and 10a are depicted in Figs. 9b and 10b, respectively, under the two cases. As shown in Fig. 9b, in the traditional DLAS, the distribution of the measured CH_4 concentration fits to a normal distribution. When the averaging time is < 109 s, the Allan deviation is proportional to $1/\mathrm{sqrt}(\tau)$, implying that the sensor was mainly dominated by White-Gaussian noise. However, the Allan deviation derived using the algorithm does not follow a $1/\mathrm{sqrt}(\tau)$ dependence, which indicates that the Gaussian white noise was suppressed and the LI-DLAS gas analyzer was mainly dominated by sensor drift. The Allan deviation of the traditional DLAS analyzer is ~ 1.514 ppmv for a 1 s averaging time. While at the same averaging time, the Allan deviation of the proposed LI-DLAS system is ~ 0.531 ppmv. Therefore, the detection stability was enhanced through the use of the LI-DLAS technique with an observation time of 1 s. With increasing the averaging time (e.g., up to > 10 s), the Allan deviation of the traditional DLAS system drops to the same level as that of the LI-DLAS system, and thus, the traditional DLAS system reveals a similar stability but at the expense of a longer measurement time than the LI-DLAS system.

Fig. 6 Flowchart of the developed C program using the proposed LI-DLAS technique for baseline fitting, Lagrangian interpolation, and nonlinear absorption line fitting shown in the dashed box. A traditional flowchart of the C program can be shown by removing the algorithm shown in the dashed box

Fig. 7 a The measured amplitude of $u_{absorbance}(t)$ for eight CH_4 concentration levels of 26, 27, 28, 30, 32, 38, 52, and 74 ppmv. **b** Experimental data dots and fitting curve of the measured CH_4 concentration versus theoretical concentration

Fig. 8 The measured absorbance of the CH_4 sample with the concentration range of 26.5–32 ppmv under the cases of **a** using the traditional DLAS and **b** using LI-DLAS, where 60 measurements were performed for one gas sample
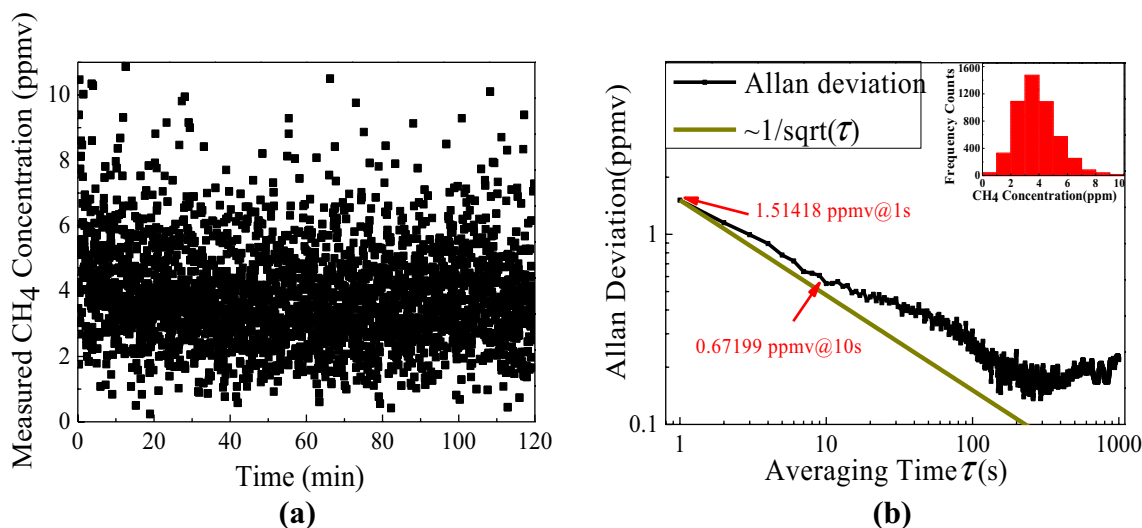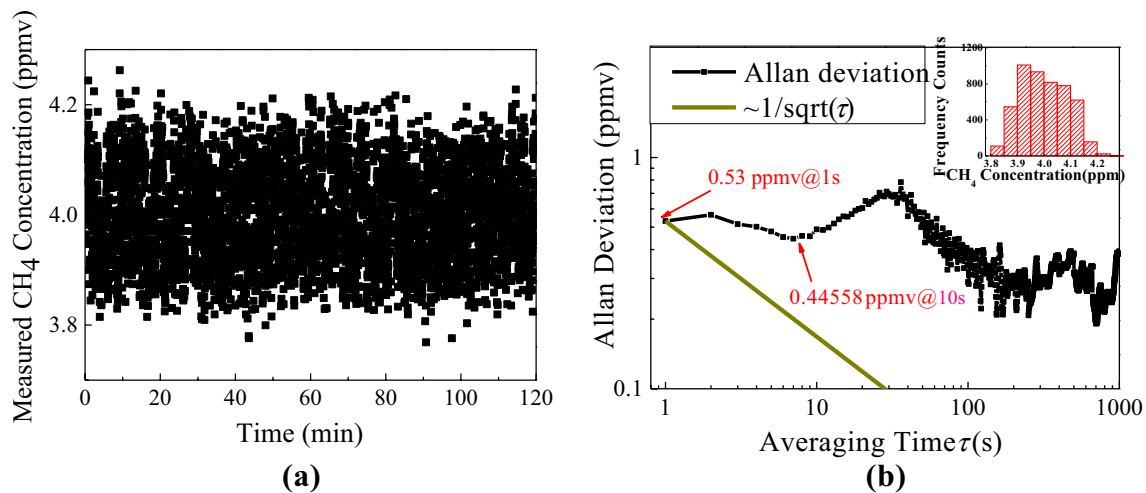

Fig. 9 **a** Measured concentration results using the traditional DLAS algorithm for a 4 ppmv CH_4 sample for ~2 h. **b** Allan deviation curve versus the averaging time τ. The inset shows the histogram plot based on the measurement results using the traditional DLAS algorithm

5 Conclusions

To suppress the electrical-domain background noise, a novel LI-DLAS analyzer for CH_4 detection was proposed by incorporating an LI data processing algorithm, a nonlinear least-square fitting (NLLSF) algorithm, and a 1654 nm distributed feedback (DFB) laser. Comparative experimental results of the traditional DLAS sensor and the developed LI-DLAS sensor prove the superiority of the LI-DLAS technique. Using the developed algorithm for Gaussian white noise suppression, the detection sensitivity was decreased from 6 to 2 ppmv, and the Allan deviation was decreased from 1.514 to 0.531 ppmv for a 1 s averaging time. Compared with the traditional DLAS analyzer based on LabVIEW platform, the DSP-based CH_4 sensor shows the merits of compact size and low cost with potential filed applications in industrial monitoring and control. Meanwhile, the demonstrated LI-DLAS sensor architecture is also applicable in other infrared gas sensing.

Fig. 10 **a** Measured concentration results using the LI-DLAS algorithm for a 4 ppmv CH_4 sample for ~2 h. **b** Allan deviation curve versus the averaging time τ. The inset shows the histogram plot based on the measurement results using the LI-DLAS algorithm

References

1. W. Ren, W.Z. Jiang, F.K. Tittel, Single-QCL-based absorption sensor for simultaneous trace-gas detection of CH_4 and N_2O. Appl. Phys. B Lasers Opt. **117**(1), 245–251 (2014)
2. C.T. Zheng, W.L. Ye, N.P. Sanchez, C.G. Li, L. Dong, Y.D. Wang, R.J. Griffin, F.K. Tittel, Development and field deployment of a mid-infrared methane sensor without pressure control using interband cascade laser absorption spectroscopy. Sens. Actuat. B Chem. **244**, 365–372 (2017)
3. W.L. Ye, C.G. Li, C.T. Zheng, N.P. Sanchez, A.K. Gluszek, A.J. Hudzikowski, L. Dong, R.J. Griffin, F.K. Tittel, Mid-infrared dual-gas sensor for simultaneous detection of methane and ethane using a single continuous-wave interband cascade laser. Opt. Express **24**(15), 16973–16985 (2016)
4. E.S.F. Berman, M. Fladeland, J. Liem, R. Kolyer, M. Gupta, Greenhouse gas analyzer for measurements of carbon dioxide, methane, and water vapor aboard an unmanned aerial vehicle. Sens. Actuat. B Chem. **169**, 128–135 (2012)
5. W.W. Ding, L.Q. Sun, L.Y. Yi, E.Y. Zhang, 'Baseline-offset' scheme for a methane remote sensor based on wavelength modulation spectroscopy. Meas. Sci. Technol. **27**(8), 085202 (2016)
6. A. Groth, C. Maurer, M. Reiser, M. Kranert, Determination of methane emission rates on a biogas plant using data from laser absorption spectrometry. Biores. Technol. **178**, 359–361 (2015)
7. N.P. Sanchez, C.T. Zheng, W.L. Ye, B. Czader, D.S. Cohan, F.K. Tittel, R.J. Griffin, Exploratory study of atmospheric methane enhancements derived from natural gas use in the Houston urban area. Atmos. Environ. **176**, 261–273 (2018)
8. M. Dong, C.T. Zheng, S.Z. Miao, Y. Zhang, Q.L. Du, Y.D. Wang, F.K. Tittel, Development and measurements of a mid-infrared multi-gas sensor system for CO, CO_2 and CH_4 detection. Sensors **17**(10), 2221 (2017)
9. A.R. Brandt, G.A. Heath, E.A. Kort, F. O'Sullivan, G. Petron, S.M. Jordaan, P. Tans, J. Wilcox, A.M. Gopstein, D. Arent, S. Wofsy, N.J. Brown, R. Bradley, G.D. Stucky, D. Eardley, R. Harriss, Energy and environment. Methane leaks from North American natural gas systems. Science **343**(6172), 733–735 (2014)
10. R.A. Alvarez, S.W. Pacala, J.J. Winebrake, W.L. Chameides, S.P. Hamburg, Greater focus needed on methane leakage from natural gas infrastructure. Proc. Natl. Acad. Sci. **109**(17), 6435–6440 (2012)
11. J. Jiang, G. M. Ma, H. T. Song, C. R. Li, Y. T. Luo, and H. B. Wang, Highly sensitive detection of methane based on tunable diode laser absorption spectrum. IEEE Conf. Int. Instrum. Measur. Technol. **26**, 104–108 (2016)
12. J.S. Li, B.L. Yu, H. Fischer, Wavelet transform based on the optimal wavelet pairs for tunable diode laser absorption spectroscopy signal processing. Appl. Spectrosc. **69**(4), 496–506 (2015)
13. J.A. Silver, Frequency-modulation absorption spectroscopy for trace species detection: theoretical and experimental comparison among methods. Appl. Opt. **31**(6), 707–717 (1992)
14. L. Dong, Y.J. Yu, C.G. Li, S. So, F.K. Tittel, Ppb-level formaldehyde detection using a CW room-temperature interband cascade laser and a miniature dense pattern multi-pass gas cell. Opt. Express **23**(15), 19821–19830 (2015)
15. H.I. Schiff, D.R. Hastie, G.I. Mackay, T. Iguchi, B.A. Ridley, Tunable diode laser systems for measuring trace gases in tropospheric air. Environ. Sci. Technol. **17**(8), 352A–364A (1983)
16. Q. X. He, C. T. Zheng, H. F. Liu, Y. D. Wang, and F. K. Tittel, A near-infrared gas sensor system based on tunable laser absorption spectroscopy and its application in CH_4/C_2H_2 detection. Proc. SPIE **10111**, 1011135-1–1011135-7 (2017)
17. B. Li, C.T. Zheng, Q.X. He, W.L. Ye, Y. Zhang, J.Q. Pan, Y.D. Wang, Development and measurement of a near-infrared CH_4, detection system using 1.654 μm wavelength-modulated diode laser and open reflective gas sensing probe. Sens Actuat B Chem **225**, 188–198 (2016)

18. F.A. Blum, K.W. Nill, P.L. Kelley, A.R. Calawa, T.C. Harman, Tunable infrared laser spectroscopy of atmospheric water vapor. Science **177**(4050), 694–695 (1972)

19. J.S. Li, B.L. Yu, W.X. Zhao, W.D. Chen, A review of signal enhancement and noise reduction techniques for tunable diode laser absorption spectroscopy. Appl. Spectrosc. Rev. **49**(8), 666–691 (2014)

20. J.S. Li, H. Deng, P.F. Li, B.L. Yu, Real-time infrared gas detection based on an adaptive Savitzky-Golay algorithm. Appl. Phys. B Lasers Opt. **120**(2), 207–216 (2015)

21. F. Zhang, J.X. Hang, S.B. Wang, Time-delay compensation method of FOG based on Lagrange interpolation. J. Chin. Inertial Technol. **25**(5), 676–680 (2017)

22. C.T. Zheng, W.L. Ye, N.P. Sanchez, A.K. Gluszek, A.J. Hudzikowski, C.G. Li, L. Dong, R.J. Griffin, F.K. Tittel, Infra-red dual-gas CH_4/C_2H_6 sensor using two continuous-wave interband cascade lasers. IEEE Photon. Technol. Lett. **28**(21), 2351–2354 (2016)

23. L.S. Rothman, I.E. Gordon, Y. Babikov, A. Barbe, D.C. Benner, P.F. Bernath, M. Birk, L. Bizzocchi, V. Boudon, L.R. Brown, A. Campargue, K. Chance, E.A. Cohen, L.H. Coudert, V.M. Devi, B.J. Drouin, A. Fayt, J.M. Flaud, R.R. Gamache, J.J. Harrison, J.M. Hartmann, C. Hill, J.T. Hodges, D. Jacquemart, A. Jolly, J. Lamouroux, R.J. Le Roy, G. Li, D.A. Long, O.M. Lyulin, C.J. Mackie, S.T. Massie, S. Mikhailenko, H.S.P. Muller, O.V. Naumenko, A.V. Nikitin, J. Orphal, V. Perevalov, A. Perrin, E.R. Polovtseva, C. Richard, M.A.H. Smith, E. Starikova, K. Sung, S. Tashkun, J. Tennyson, G.C. Toon, V.G. Tyuterev, G. Wagner, The Hitran 2012 molecular spectroscopic database. J. Quant. Spectrosc. Radiat. Transfer **130**, 4–50 (2013)

24. The HITRAN Database. https://www.cfa.harvard.edu/hitran/. Accessed 6 Aug 2018

25. R.K. Hanson, R.M. Spearrin, C.S. Goldenstein, *Spectroscopy and optical diagnostics for gases* (Springer, Berlin, 2016)

26. C. Claveau, A. Henry, D. Hurtmans, A. Valentin, Narrowing and broadening parameters of H_2O lines perturbed by He, Ne, Ar, Kr and nitrogen in the spectral range 1850–2140 cm^{-1}. J. Quant. Spectrosc. Radiat. Transfer **68**(3), 273–298 (2001)

27. A. Valentin, Ch. Claveau, A.D. Bykov, N.N. Lavrentieva, V.N. Saveliev, L.N. Sinitsa, The water-vapor ν2 band lineshift coefficients induced by nitrogen pressure. J. Mol. Spectrosc. **198**(2), 218–229 (1999)

28. D.E. Heard, *Analytical techniques for atmospheric measurement* (Blackwell Publishing, Oxford, 2006)

29. G.C. Xiong, Adaptive Filter. Geophys. Geochem. Explor. **22**(2), 147–153 (2000)